

# Ultra-Close Tidal Disruption Events with Prompt Hyperaccretion

A Thesis  
Presented to  
The Academic Faculty

by

**Christopher Evans**

In Partial Fulfillment  
of the Requirements for the Degree  
Bachelors of Science in the School of Physics

School of Physics  
Georgia Institute of Technology  
May 2015

Copyright © 2015 by Christopher Evans

# Ultra-Close Tidal Disruption Events with Prompt Hyperaccretion

Approved by:

Professor Pablo Laguna  
School of Physics

Professor Deirdre Shoemaker  
School of Physics

Professor Brian Kennedy  
School of Physics

## ACKNOWLEDGEMENTS

I would like to deeply thank Professors Pablo Laguna and Deirdre Shoemaker for their endless help and guidance throughout this research project. I also thank Michael Clark and Dr. Tanja Bode for their help in making me familiar with our the previously existing code and tidal disruption events in general. Additionally I thank Professor Tamara Bogdanović and Professor Mike Eracelous for beneficial comments and discussions. Finally, and most importantly, I thank Karissa, Shannon, and my mother, father, brother and grandmother for their endless love and support throughout my time as an undergraduate.

This work was supported by NSF grants 1205864, 1212433, 1333360. Computations at XSEDE TG-PHY120016 and the Cygnus cluster at Georgia Tech.

# TABLE OF CONTENTS

ACKNOWLEDGEMENTS . . . . .	iii
LIST OF TABLES . . . . .	v
LIST OF FIGURES . . . . .	vi
ABSTRACT . . . . .	1
I INTRODUCTION . . . . .	2
II CANONICAL TIDAL DISRUPTIONS AT A GLANCE . . . . .	6
III NEW TDE REGIME . . . . .	10
IV ANATOMY OF A DISRUPTION . . . . .	12
V RESULTS . . . . .	14
VI CONCLUSIONS . . . . .	18

# LIST OF TABLES

3.1	Simulation Parameters and Accretion Rates. . . . .	10
-----	--	----

# LIST OF FIGURES

2.1	Domain of astrophysical relevance of tidal disruptions for a main-sequence star with mass $M_* = M_\odot$ and radius $R_* = R_\odot$ . The thick vertical line denotes canonical TDEs. The square point shows the ultra-close TDE from [1] and crosses those in the present study. . . . .	7
4.1	BH accretion rate as a function of time. Panels A, B and C display cases with penetration factor $\beta = 10$ grouped by the spin parameter of the BH in order to assess the effect of the mass of the star, $a/M_h = 0, -0.65$ and $0.65$ correspond to panels A, B and C, respectively. Panels D and E display the accretion rates for the star with a mass $M_* = 0.57 M_\odot$ for penetration factor $\beta = 10$ (panel D) and $\beta = 15$ (panel E). . . . .	13
5.1	Snapshots of the density (top), temperature (middle), and specific entropy (bottom) of the debris at $t = -28s$ , $t = 450s$ , and $t = 1250s$ for the run $\beta_{10}S_0M_{0.57}$ . . . . .	14
5.2	Histograms of the mass per unit binding energy at times $t = -28s$ , $t = 450s$ , and $t = 1250s$ for the case shown in Figure 5.1. . . . .	16

# ABSTRACT

A bright flare from a galactic nucleus followed at late times by a  $t^{-5/3}$  decay in luminosity is often considered to be the signature of a tidal disruption of a star by a massive black hole. The flare and afterglow are produced when the stream of stellar debris released by the disruption returns to the vicinity of the black hole, self-intersects, and eventually forms an accretion disk or torus. In the canonical scenario of a solar-type star disrupted by a  $10^6 M_\odot$  black hole, the time between the disruption of the star and the formation of the accretion torus could be years. Presented here are fully general relativistic simulations of a new class of tidal disruption events involving ultra-close encounters of solar-type stars with intermediate mass black holes. In these encounters, a thick disk forms promptly after disruption, on timescales of hours. After a brief initial flare, the accretion rate remains steady and highly super-Eddington for a few days at  $\sim 10^2 M_\odot \text{yr}^{-1}$ .

# CHAPTER I

## INTRODUCTION

While evidence supporting the presence of black holes (BHs) at the center of most galaxies is mounting, still more methods for the identification of these objects are needed to cover larger potential mass ranges for the BHs. This is particularly important in quiescent galaxies wherein accretion powered nuclear activity is absent, and as a result they are not highly luminous. Lacking this activity, the electromagnetic signatures of tidal disruption events (TDEs) should be distinguishable.

As more potential observations accumulate, simulations that expand the well understood parameter space become necessary to interpret these observations. We have identified a region of TDE parameter space that displays prompt hyperaccretion and torus formation. The accretion rate data of this study can be used to widen understanding of potential observational signatures of TDEs, and hopefully guide astronomical searches.

Interest in TDEs was sparked in the 1970s with the suggestion that some active galactic nuclei (AGN) could contain massive BHs. It was hypothesized by Hills in 1975 that TDEs could provide both the required matter to fuel the growth of the massive BH, and the mass accretion that leads to the observed luminosity of AGN [2]. Hills made some preliminary calculations regarding the growth rate of massive BHs that undergo TDEs, and the resultant luminosities. While these calculations were Newtonian and very approximate, they provide a good starting point. He also pointed out that for BHs with a mass  $M > 3 \times 10^8 M_\odot$ , the radius within which tidal disruption takes place (tidal radius) is less than the Schwarzschild radius, and therefore stars are either not disrupted (if they pass far enough from the black hole), or completely absorbed. Following this, he calculated the stellar mass density required in the area around the BH for it to grow from a mass consistent with stellar evolution into a massive BH ( $M \simeq 10^8 M_\odot$ ). At this point however, TDEs were still not very well understood, so these results were preliminary, at best.

In the 1980s, more evidence gathered for a concentrated dark mass at the galactic center [3], which increased curiosity in TDEs leading to a comprehensive qualitative study of TDEs by Rees in 1988 [4]. This study was more focused on the resultant debris from a TDE. Previously it had been assumed that the majority of the matter from the disruption would be gravitationally bound to the BH and eventually accreted. Rees noted however that before reaching periastron the star will develop a quadrupole distortion which results in a gravitational torque. This causes a significant angular velocity in the star that is aligned with the orbital angular momentum. As such, when the star reaches periastron, the gas on the part of the star furthest from the black hole will have an increased total velocity (and consequently orbital energy) relative to the BH, and the closer gas will have a diminished total velocity. This creates a very large spread in orbital energies, which results in (under Rees' simplifying assumption that the orbital energy distribution is roughly uniform centered on zero) half of the material being bound and half unbound. While this assumption is not exactly correct in that the orbital energy distribution will likely not be uniform, this analysis captures the important idea that due to this co-rotational spin up, there will be a large spread in the orbital energies resulting in both bound and unbound material.

Due to the large spread in orbital energies, some of the unbound material can be ejected at very high speed. Rees also argues that the bound material will accrete rather quickly due to viscous effects and shocks resulting from relativistic orbital effects. Possibly one of the most important results of this study is that accretion rate (and consequently the luminosity) resulting from this disc of bound material will fall off as  $t^{-5/3}$ , which potentially provides a way to identify tidal disruption events from the decay of an observed electromagnetic signature.

Rees also notes that for ultraclose passages (such as those that are the subject of our study) for which the pericentric distance is much smaller than the tidal radius, relativistic effects are dynamically significant. This put a very clear bound on the applicability of early numerical simulations. Any study that wished to investigate ultraclose passages could not make a Newtonian approximation without producing erroneous results.

Shortly following this qualitative description of TDEs was one of the first numerical

studies presented by Evans and Kochanek [5]. In order to not overstep current computational bounds, this study investigated the regime in which the pericentric distance is equal to the tidal radius. Under these conditions the star is still disrupted, however the tidal fields are sufficiently weak, and thus a Newtonian approximation can be made with reasonable accuracy. This study also made use of smoothed particle hydrodynamics (SPH), which calculates hydrodynamic evolution using a number of discrete fluid particles [6]. In this very limited weak field regime, the results of the study matched very well with the analysis given by Rees.

In order to investigate the highly relativistic regime of close encounters, Laguna et al. made a study that involved penetration factors ( $\beta$  which is defined as the ratio of the tidal radius to the pericentric distance) as high as 10 [1]. In this study, they utilized an implementation of SPH that evaluates the fluid particle Lagrangian on the static curved spacetime of the BH. While this is only an approximation, as the fluid self gravity is still Newtonian and the spacetime remains completely static, it is reasonably accurate for situations (such as this) where the BH is by far the major source of curvature. These simulations demonstrated key relativistic effects as a result of orbital precession, such as the possibility of a parabolic orbit crossing itself.

Subsequent studies have incorporated detailed micro-physics [7, 8, 9], considered a wider variety of stellar objects, such as white-dwarfs and red-giants [10, 11, 12, 9, 13], covered longer dynamical times [14], and included better descriptions of gravity for ultra-close encounters [1, 15, 16].

A challenging aspect of TDE studies is the inherent difficulty in capturing numerically the formation of the accretion disk from the bound stellar debris [17, 18, 19, 20]. The complication arises because, in canonical TDEs, the time between the disruption of the star and the formation of the accretion disk amounts to several orbital periods of the stellar debris that are in highly eccentric orbits. This translates into years for a solar-type star disrupted by a  $10^6 M_\odot$  BH. For reference, numerical simulations in these cases cover at most a few tens of hours.

In a series of very recent papers, circularization of the returning debris is addressed

with a variety of methods. Shiokawa et al. find that the debris circularizes at a larger radius than previously thought and that the accumulation of mass in the ensuing ring is fairly slow (the characteristic time scale is several times the orbital period of the most tightly bound debris) [21]. Guillochon and Ramirez-Ruiz consider the self-intersection of thin post-disruption streams for an ensemble of events and conclude that streams *typically* self-intersect at large distances from the BH, leading to a long viscous time and an extensive delay before the onset of rapid accretion [22]. Bonnerot et al. and Hayasaki et al. point out the importance of cooling on the rate of circularization of the debris; their general conclusion is that efficient cooling leads to very long circularization time scales, hence a delay in the onset of accretion [23, 24]. The picture emerging from the studies above is that, although accretion could be prompt under the right conditions, it is likely that the onset of accretion is delayed by an appreciable amount of time, perhaps of order a year.

Our study introduces examples of a new class of TDEs, for which a puffed disk or torus forms promptly after disruption. Furthermore, the BH accretes at a steady and highly super-Eddington rate of about  $10^2 M_{\odot} \text{yr}^{-1}$ . The TDEs in our study involve ultra-close encounters between low mass ( $0.57 - 1 M_{\odot}$ ) stars and a  $10^5 M_{\odot}$  BH. TDEs with intermediate mass BHs, but larger separation encounters, have been also studied by Ramirez-Ruiz and Rosswog [25]. Our simulations are in a regime where accounting for full general relativistic effects is needed, including those from the spin of the BH. In these ultra-close encounters, the star is effectively disrupted as it arrives at periapsis, with the tidal debris plunging into the BH almost instantaneously (on the timescale of one orbital period). Moreover, as a result of the extreme proximity of the debris to the BH, general relativistic precession is very efficient in circularizing stellar material to form an expanding torus that engulfs the BH. The inner material in the torus spirals into the BH and is accreted at a constant rate until the supply of bound debris is exhausted.

## CHAPTER II

### CANONICAL TIDAL DISRUPTIONS AT A GLANCE

A star of mass  $M_*$  and radius  $R_*$  interacting with a BH of mass  $M_h$ , likely in a highly eccentric or parabolic orbit [26, 27, 28], will be disrupted by tidal forces if the star approaches near the BH within a distance  $R_t$ , called the *tidal radius*, given approximately by

$$R_t \equiv R_* \left( \frac{M_h}{M_*} \right)^{1/3}. \quad (2.1)$$

Denoting the distance of closest approach to the BH as  $R_p$ , it is customary to characterize the strength of a TDE encounter by the *penetration factor*  $\beta$ , which is defined as

$$\beta \equiv \frac{R_t}{R_p} = \frac{R_*}{R_p} \left( \frac{M_h}{M_*} \right)^{1/3}. \quad (2.2)$$

The fourth length scale in the problem, in addition to  $R_*$ ,  $R_t$  and  $R_p$ , is the gravitational radius  $R_g = G M_h / c^2$ , which is equal to half the horizon radius for a non-spinning BH and the full horizon radius for a maximally rotating BH.

Given  $R_*$ ,  $R_t$ ,  $R_p$  and  $R_g$ , it is illustrative to pictorially represent the domain of astrophysical relevance of TDEs, as first suggested by Luminet and Pichon [29]. One such representation of this domain is a triangle in the  $\beta$  vs  $M_h$  diagram as shown in Figure 2.1. Interpreting  $\beta$  in Eq. (2.2) as a function of  $R_p$  clarifies the demarcations between different regions of parameter space. The base of the triangle is  $R_p = R_t$ , or  $\beta_t \equiv \beta(R_t) = 1$ . Below this line ( $R_p > R_t$ ) it is clear that there is no disruption. The left side of the triangle is the line obtained by setting  $R_p = R_*$ ; that is,

$$\beta_* \equiv \beta(R_*) = \left( \frac{M_h}{M_*} \right)^{1/3}. \quad (2.3)$$

To the left of this line ( $R_p < R_*$ ) lie very close encounters where *the BH enters the star* in the process of disrupting it. The process is very similar to the high-speed collisions of stellar-mass BHs and red giants as studied by Dale et al. [30]. Finally, the right side of the

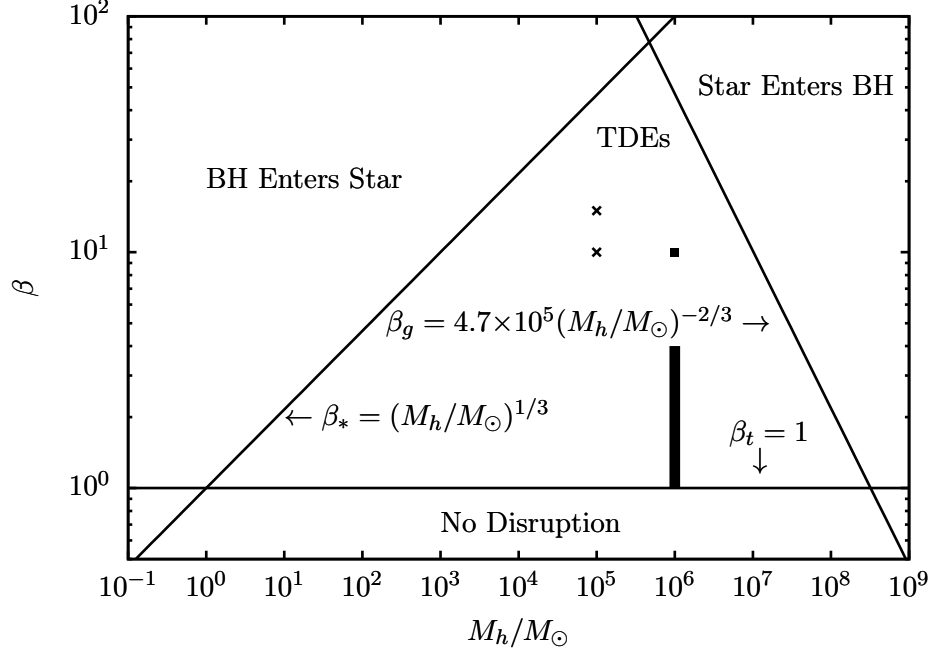


**Figure 2.1:** Domain of astrophysical relevance of tidal disruptions for a main-sequence star with mass  $M_* = M_\odot$  and radius  $R_* = R_\odot$ . The thick vertical line denotes canonical TDEs. The square point shows the ultra-close TDE from [1] and crosses those in the present study.

triangle is the line when  $R_p = R_g$ ; that is,

$$\beta_g \equiv \beta(R_g) = \frac{R_*}{G M_* / c^2} \left( \frac{M_h}{M_*} \right)^{-2/3}. \quad (2.4)$$

To the right of this line ( $R_p < R_g$ ) are events where the *star enters the BH* before it is disrupted.

According to Figure 2.1, for a sun-like star ( $M_* = M_\odot$  and  $R_* = R_\odot$ ), the maximum BH mass to disrupt the star is  $M_h = 3.2 \times 10^8 M_\odot$ . Additionally, the highest penetration factor for which disruption can take place is  $\beta = 78$ , which involves a  $M_h = 4.7 \times 10^5 M_\odot$  BH. The edges of the triangle of astrophysical relevance are, of course, not sharp due to variations in the definition of relevant length scales arising from the spin of the BH, the space-time curvature in the neighborhood of the BH, and the internal structure of the star.

After disruption, the receding debris spreads, with roughly half of the material remaining

bound to the BH. The most bound material has specific binding energy given by

$$\begin{aligned} e_{\min} &\simeq -\frac{G M_h \Delta R_*}{R_f^2} \\ &\simeq -G \beta^2 f^{-2} \xi M_*^{2/3} R_*^{-1} M_h^{1/3}, \end{aligned} \quad (2.5)$$

where  $\Delta R_* = \xi R_*$  is the spread of the debris with  $\xi$  being a deformation factor, and

$$R_f = R_t \left[ \frac{\beta n + (1 - n)}{\beta} \right] = \frac{R_t f(\beta, n)}{\beta} \quad (2.6)$$

is the distance to the BH when the spread in specific binding energy of the debris freezes-in. In the original estimates [5]  $n = 0$  ( $f = 1$ ), and thus  $R_f = R_p$ . More recent studies [31, 8] suggest that  $n = 1$  ( $f = \beta$ ), so  $R_f = R_t$ . In our study, we observed that  $n \sim 0.5$ , which for large  $\beta$  translates into  $f \sim 0.5$ .

With  $e_{\min}$  at hand, the characteristic fallback time for the most tightly bound material to return to the BH is

$$\begin{aligned} t_{\min} &\simeq 2\pi \frac{G M_h}{(2|e_{\min}|)^{3/2}} \\ &\simeq \frac{\pi}{\sqrt{2G}} \beta^{-3} f^3 \xi^{-3/2} R_*^{3/2} M_*^{-1} M_h^{1/2}. \end{aligned} \quad (2.7)$$

An estimate of the debris return at late times is obtained from the Keplerian relation

$$\frac{de}{dt} = \frac{1}{3} (2\pi G M_h)^{2/3} t^{-5/3} \quad (2.8)$$

and the mass per specific binding energy

$$\frac{dM_h}{de} \simeq \frac{M_*}{2|e_{\min}|} \simeq \frac{M_*}{t_{\min}^{-2/3} (2\pi G M_h)^{2/3}}, \quad (2.9)$$

which is assumed to be roughly constant. Therefore,

$$\dot{M}_h \equiv \frac{dM_h}{dt} = \frac{dM_h}{de} \frac{de}{dt} \simeq \dot{M}_{\max} \left( \frac{t}{t_{\min}} \right)^{-5/3}. \quad (2.10)$$

with  $\dot{M}_{\max} \equiv M_*/(3t_{\min})$ . The power-law decay of  $t^{-5/3}$  in Eq. (2.10) is considered to be a ubiquitous property of TDEs as long as the mass per unit binding energy of the debris is approximately constant [26, 5, 1, 9]. Slight departures from this power-law have been found close to the peak accretion rate as a result of the equation of state of the star [7] or effects

from the spin of the BH [11]. Recent work by Guillochon and Ramirez-Ruiz has shown that the canonical  $t^{-5/3}$  is only characteristic of full tidal disruptions [8].

In the case of a TDE with  $M_* = M_\odot$ ,  $R_* = R_\odot$  and  $M_h = 10^6 M_\odot$ ,

$$t_{\min} \simeq 0.11 \beta^{-3} f^3 \xi^{-3/2} r_*^{3/2} m_*^{-1} M_6^{1/2} \text{ yr}, \quad (2.11)$$

and

$$\dot{M}_{\max} \simeq 0.3 \beta^3 f^{-3} \xi^{3/2} r_*^{-3/2} m_*^2 M_6^{-1/2} M_\odot \text{ yr}^{-1}, \quad (2.12)$$

where  $M_6 \equiv M_h/10^6 M_\odot$ ,  $r_* \equiv R_*/R_\odot$  and  $m_* \equiv M_*/M_\odot$ . For comparison, the Eddington accretion rate in this situation is  $\dot{M}_{\text{Edd}} = 0.02 M_6 M_\odot \text{ yr}^{-1}$  (assuming 10% efficiency).

## CHAPTER III

### NEW TDE REGIME

We are interested in TDEs with  $\beta = 10$  and  $15$ , involving a BH with mass  $M_h = 10^5 M_\odot$ . They are denoted by crosses in Figure 2.1 and are closer to the *BH-enters-star* boundary than the “canonical” scenarios of  $\beta = \text{few}$  and  $M_h = 10^6 M_\odot$ , which are denoted by a thick vertical line in Figure 2.1. In the same figure, the square point shows the ultra-close TDE from [1]. We consider non-spinning BHs and BHs with spin  $a/M_h = \pm 0.65$ . The sign denotes whether the spin of the BH is aligned (plus) or anti-aligned (minus) with the orbital angular momentum of the star. The disruptions involve main-sequence type stars with masses  $M_* = 1 M_\odot$  and  $0.57 M_\odot$ , modeled as polytropes with index  $\Gamma = 4/3$  and injected in parabolic orbits. Table 3.1 provides the parameters of the simulations: the penetration factor  $\beta$ , the BH spin parameter  $a$ , and the mass of the star  $M_*$ . The simulations fully account for general relativistic effects. To this end, we use our numerical relativity infrastructure Maya, used also in our previous general relativistic TDE studies [11].

**Table 3.1:** Simulation Parameters and Accretion Rates.

Run	$\beta$	$a/M_h$	$M_*/M_\odot$	$M_{\max} (M_\odot \text{ yr}^{-1})$	$M_{\text{late}}(M_\odot \text{ yr}^{-1})$
$\beta_{10}S_0M_1$	10	0	1	$3.6 \times 10^2$	$1.0 \times 10^3$
$\beta_{10}S_{0.65}M_1$	10	0.65	1	$1.0 \times 10^4$	$7.5 \times 10^2$
$\beta_{10}S_{-0.65}M_1$	10	-0.65	1	$1.2 \times 10^5$	$2.0 \times 10^2$
$\beta_{10}S_0M_{0.57}$	10	0	0.57	$3.5 \times 10^2$	$1.0 \times 10^2$
$\beta_{10}S_{0.65}M_{0.57}$	10	0.65	0.57	$7.6 \times 10^3$	$4.0 \times 10^2$
$\beta_{10}S_{-0.65}M_{0.57}$	10	-0.65	0.57	$7.9 \times 10^4$	$3.0 \times 10^2$
$\beta_{15}S_0M_{0.57}$	15	0	0.57	$2.0 \times 10^4$	$4.0 \times 10^2$
$\beta_{15}S_{0.65}M_{0.57}$	15	0.65	0.57	$8.8 \times 10^4$	$3.5 \times 10^2$
$\beta_{15}S_{-0.65}M_{0.57}$	15	-0.65	0.57	$3.8 \times 10^5$	$2.0 \times 10^2$

In general terms, the TDEs studied here involve stars comparable in size to the BH,  $R_* \simeq 4.7 M_5^{-1} r_* R_g$ , periapsis distances of about

$$R_p \simeq 4.64 \beta_{10}^{-1} M_5^{1/3} m_*^{-1/3} R_*, \quad (3.1)$$

and tidal radius

$$R_t \simeq 218 M_5^{-2/3} m_*^{-1/3} r_* R_g, \quad (3.2)$$

where  $M_5 \equiv M_h/10^5 M_\odot$  and  $\beta_{10} \equiv \beta/10$ . Although the value of  $R_p$  suggests that the star could potentially swing by the BH without the BH entering the star, the combination of large  $\beta$  and general relativistic effects produce an outcome dramatically different from the situations with  $\beta \sim 1$  and  $10^6 M_\odot$  mass BHs (next section).

With  $\beta \geq 10$  and intermediate mass BHs, the star will be effectively disrupted and stretched to a few times its original size by the time it reaches periaapsis passage. A deformation factor  $\xi \simeq 4$  was found to be common in our simulations. Therefore, from Eqs. (2.7) and (2.10)

$$t_{\min} \simeq 137 \beta_{10}^{-3} f^3 \xi_4^{-3/2} r_*^{3/2} m_*^{-1} M_5^{1/2} \text{ s}, \quad (3.3)$$

and

$$\dot{M}_{\max} \simeq 9.6 \times 10^3 \beta_{10}^3 f^{-3} \xi_4^{3/2} r_*^{-3/2} m_*^2 M_5^{-1/2} M_\odot \text{ yr}^{-1}, \quad (3.4)$$

where  $\xi_4 = \xi/4$ . For reference, the Eddington accretion rate in this case is  $\dot{M}_{\text{Edd}} = 0.002 M_5 M_\odot \text{ yr}^{-1}$ . Our simulations show that  $\dot{M}_{\max} \sim 10^4 M_\odot \text{ yr}^{-1}$  and  $t_{\min} \sim 25$  s. This time-scale is comparable to the circular orbital period of the most bound material:

$$\begin{aligned} P_{\text{circ}} &= 2\pi \sqrt{\frac{(R_p - \Delta R_*)^3}{G M_h}} \\ &\simeq 316 (1 - \Delta R_*/R_p)^{3/2} \beta_{10}^{-3/2} r_*^{3/2} m_*^{-1/2} \text{ s} \\ &\simeq 16.5 \beta_{10}^{-3/2} r_*^{3/2} m_*^{-1/2} \text{ s}, \end{aligned} \quad (3.5)$$

where  $\Delta R_*/R_p \simeq 0.86 \xi_4 \beta_{10} m_*^{1/3} M_5^{1/3}$ .

## CHAPTER IV

### ANATOMY OF A DISRUPTION

We focus this discussion chiefly on the accretion rates onto the BH. Figure 4.1 shows the accretion rates of tidal debris through the BH horizon. The time axis is such that  $t = 0$  denotes periapsis passage. Three distinct accretion epochs or stages are identifiable in most of the cases.

The first phase is a narrow spike or flare in the accretion rate. The spike is due to the portion of the stellar debris that immediately plunges into the BH. An estimate of this accretion rate is given by

$$\begin{aligned}\dot{M}_h &\sim A_h \rho_\infty v_\infty \\ &\sim 10^4 \beta_{10}^{1/2} M_5^{7/3} m_*^{7/6} r_*^{-7/2} M_\odot \text{yr}^{-1},\end{aligned}\tag{4.1}$$

where we have used  $A_h \sim 4\pi R_g^2$ ,  $v_\infty \sim (GM_h/R_p)^{1/2}$  and  $\rho_\infty \sim M_*/(4\pi R_*^3/3)$ . This estimate is consistent with the values for  $\dot{M}_{\text{max}}$  reported in Table 3.1.

The next stage following the accretion flare is a decay phase, which for the simulations involving a non-spinning BH as seen in Figure 4.1 (top panel), loosely resembles a power-law decay. The duration and the presence of this decay seem to depend on the spin of the BH and the penetration factor  $\beta$ .

Finally, as new material returns to the BH, it circularizes and forms an accretion torus on a timescale of  $\sim 10 t_{\text{min}} \sim 1,400$  s [5], with the accretion eventually reaching steady state at about  $\dot{M}_{\text{late}} \sim 10^2 M_\odot \text{yr}^{-1}$ , as noted in the last column of Table 3.1. The steady state accretion will cease when the mass supply from the bound debris is depleted. Our simulations do not last long enough to reach this regime.

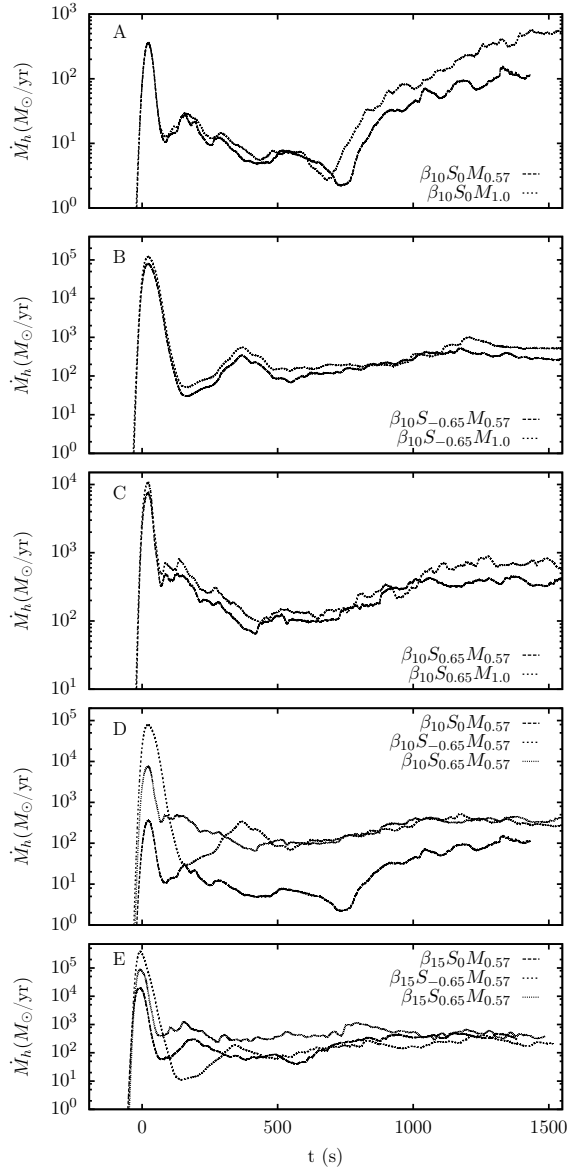


**Figure 4.1:** BH accretion rate as a function of time. Panels A, B and C display cases with penetration factor  $\beta = 10$  grouped by the spin parameter of the BH in order to assess the effect of the mass of the star,  $a/M_h = 0, -0.65$  and  $0.65$  correspond to panels A, B and C, respectively. Panels D and E display the accretion rates for the star with a mass  $M_* = 0.57 M_\odot$  for penetration factor  $\beta = 10$  (panel D) and  $\beta = 15$  (panel E).

# CHAPTER V

## RESULTS

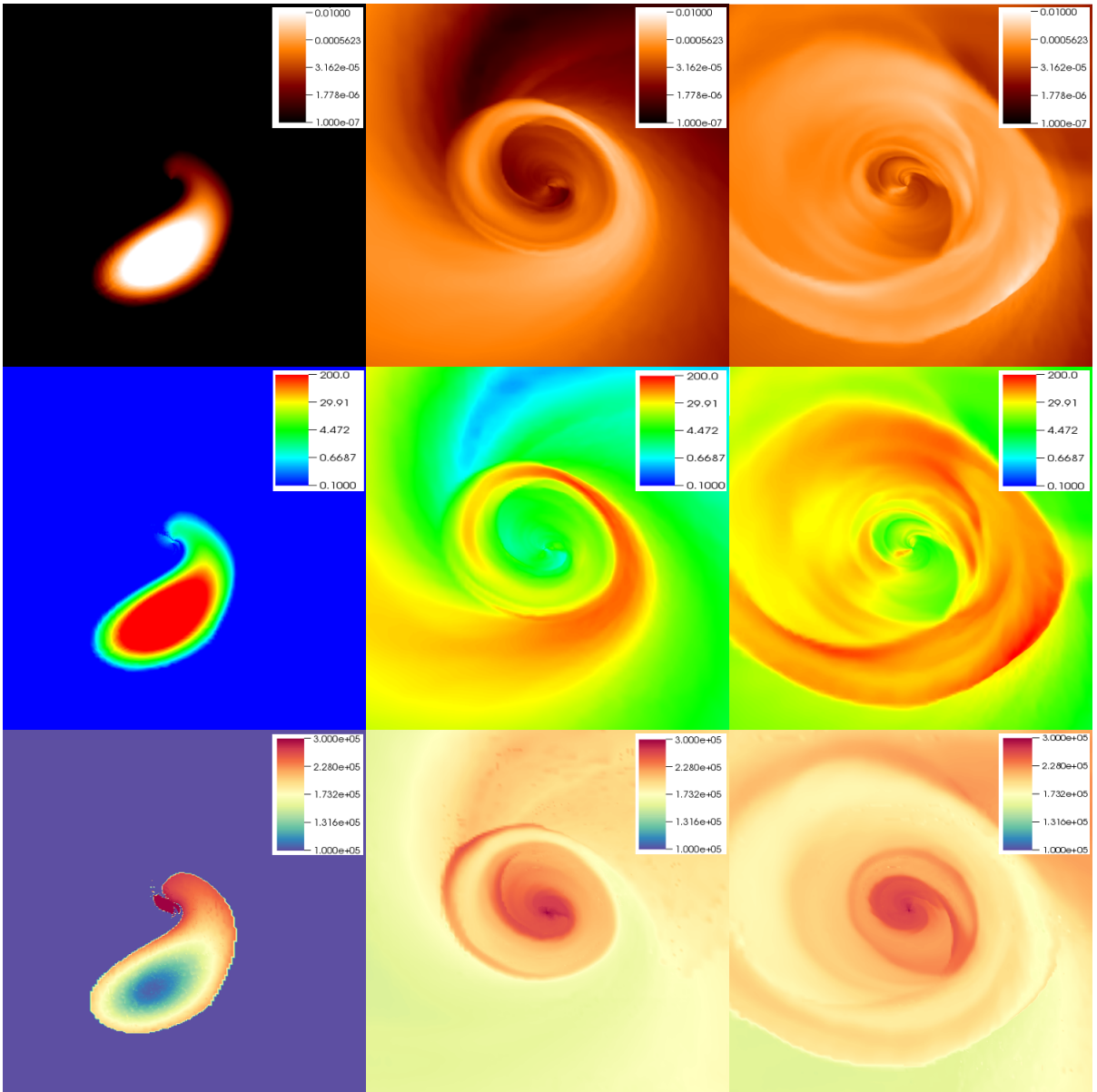


**Figure 5.1:** Snapshots of the density (top), temperature (middle), and specific entropy (bottom) of the debris at  $t = -28s$ ,  $t = 450s$ , and  $t = 1250s$  for the run  $\beta_{10}S_0M_{0.57}$ .

We report results from nine simulations, with parameters summarized in Table 3.1. To

illustrate the effect of the mass of the star, panels A, B and C in Figure 4.1 show the BH accretion rate for  $\beta = 10$ , grouping the cases with the same BH spin parameter. Notice that the accretion rate seems to be insensitive to the mass of the star. Perhaps the only case with noticeable differences is that of vanishing BH spin. We will thus focus the discussion on the star with mass  $M_* = 0.57 M_\odot$  since we have a wider variety of simulations for this star.

In panels D and E of Figure 4.1, we organize the runs according to the penetration factor, with  $\beta = 10$  in panel D and  $\beta = 15$  in panel E. Notice that the peak accretion rate of the flare is higher if the BH is spinning. Interestingly, the case with a counter-rotating orbit (i.e. BH spin anti-aligned with the orbital angular momentum) yields the largest peak accretion rate. For the  $\beta = 10$  simulations, the post-flare accretion rate depends on the BH spin magnitude but not its orientation, which is consistent with similar findings for the steady-state, subsonic accretion onto a moving BH [32]. The late-time accretion rate seems to increase with the spin of the BH. Another difference between the  $a/M_h = 0$  and the  $a/M_h = \pm 0.65$  cases is that for the latter, the time scale for flare decay is shorter; that is, the late constant accretion phase, which signals the formation of the torus, is reached after a couple of hundred seconds.

The corresponding  $\beta = 15$  cases show that the spin of the BH does not play a role in determining the late-time, constant accretion rate. Furthermore, as with the  $\beta = 10$  cases with spinning BHs, the constant accretion phase is reached within a few hundred seconds. For both the  $\beta = 10$  and  $\beta = 15$  cases, the late-time accretion rate is of the order of  $10^2 M_\odot \text{yr}^{-1}$ .

In summary, given the parameters that we varied ( $M_*$ ,  $a/M_h$ ,  $\beta$ ) and the region of parameter space that we explored, we found that the accretion rate is not very sensitive to  $M_*$ , and that the rate reached during the flare depends on both  $a/M_h$  and  $\beta$ . Furthermore, the late accretion rate for  $\beta = 15$  is not sensitive to the spin of the BH, and for both penetration factors is approximately  $\dot{M}_h \sim 10^2 M_\odot \text{yr}^{-1}$ . With the exception of the cases with  $\beta = 10$  and  $a/M_h = 0, 0.65$  (panels A and B in Figure 4.1), there are no hints of a power-law decay rate.

Figure 5.1 shows snapshots of the density, temperature, and specific entropy of the material. The top row shows the density, the middle row the temperature, and the bottom row the specific entropy, all in the orbital plane. All snapshots are from the case  $\beta_{10}S_0M_{0.57}$ , and from left to right in Figure 5.1 are at times  $t = -28s$ ,  $t = 450s$ , and  $t = 1250s$ . Both the self-intersection of stellar debris and the consequent formation of the accretion torus are evident in these snapshots.

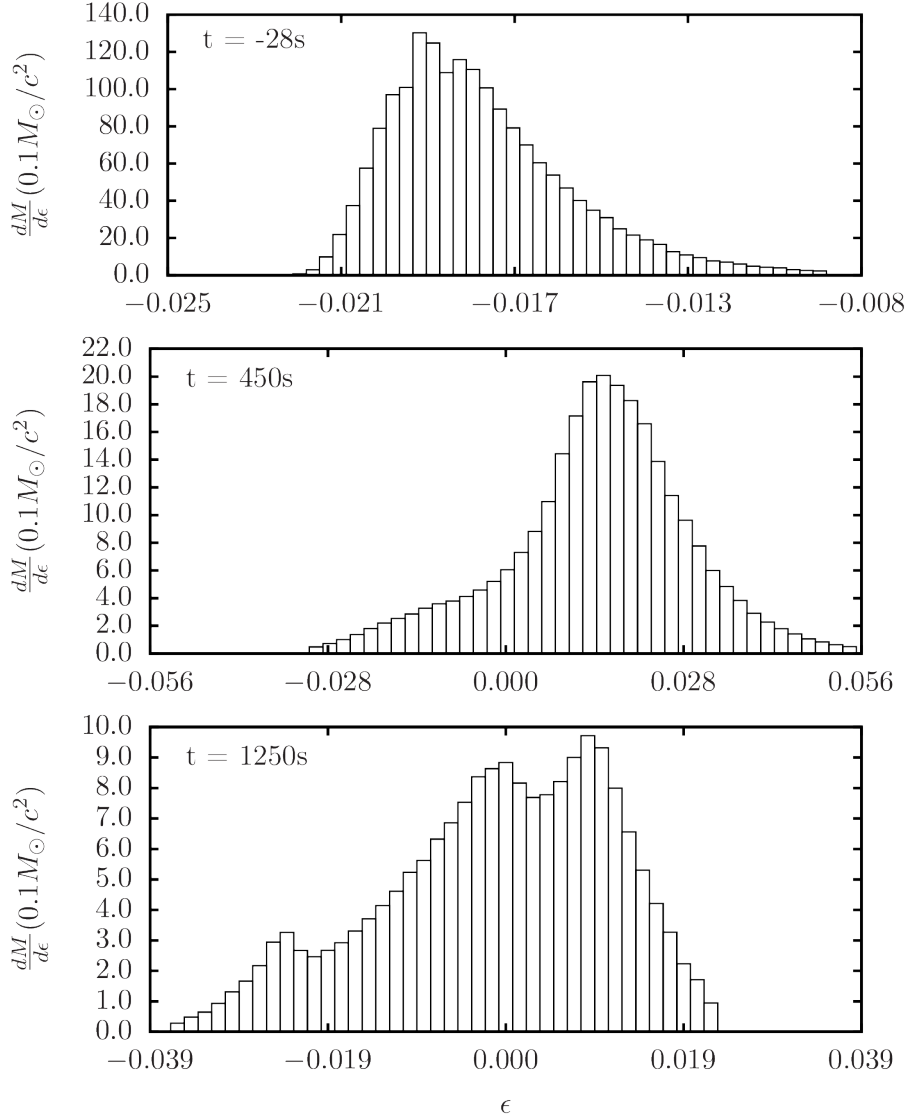


**Figure 5.2:** Histograms of the mass per unit binding energy at times  $t = -28s$ ,  $t = 450s$ , and  $t = 1250s$  for the case shown in Figure 5.1.

Additionally, there is no evidence of a  $t^{-5/3}$  decay in the accretion rates. The reasons for this are two-fold. First, since these interactions are highly relativistic, there is no reason to believe that the bound material should remain on Keplerian orbits. As such, it is not a reasonable approximation to state that  $\frac{de}{dt} \sim t^{-5/3}$ . Additionally, as can be seen in Figure 5.2, the mass per unit binding energy is not even approximately constant for these encounters.

## CHAPTER VI

### CONCLUSIONS

We presented a new class of TDEs showing prompt formation of an accretion torus after disruption and hyperaccretion. These TDEs involve ultra-close encounters with  $M_h = 10^5 M_\odot$  BH. The accretion rates of tidal material are highly super-Eddington. Additionally, there is little evidence of a  $t^{-5/3}$  decay in the accretion rate. This is likely due the strong influence of general relativistic effects in these ultra-close encounters. The late-time accretion rate, once the torus has formed, reaches an approximate steady-state and remains highly super-Eddington at  $\dot{M}_{\text{late}} \sim 10^2 M_\odot \text{ yr}^{-1}$ . With this rate, the BH should be able to accrete the majority of the bound tidal debris in just a few days. A word of caution is needed regarding the accretion rate quotes in this study. Our simulations did not include effects from radiation, which could potentially decrease the rates. However, it is not likely that radiation effects would diminish the rates enough to make them sub-Eddington, since the Eddington rate in these situations is  $\dot{M}_{\text{Edd}} = 0.002 M_5 M_\odot \text{ yr}^{-1}$  (assuming 10% efficiency).

In a subsequent study, we will expand the parameter space of our simulations and investigate the emission properties of the tidal debris. In light of the results of recent papers cited in the introduction regarding the circularization of post-disruption debris, it will be important to investigate further the role of shocks in heating and circularizing the debris as well as the overall role of cooling effects. Moreover, we will consider inclined orbits relative to the spin axis of the BH in order to compare our results with those of [17]. We are also interested in the possibility of amplification of magnetic fields and whether the class of TDEs in the present study could provide an explanation for jetted events, such as Swift J1644+57 [33, 34].

## REFERENCES

- [1] P. Laguna, W. A. Miller, W. H. Zurek, and M. B. Davies. Tidal disruptions by supermassive black holes - Hydrodynamic evolution of stars on a Schwarzschild background. *Ap. J. Lett.*, 410:L83–L86, June 1993.
- [2] J. G. Hills. Possible power source of Seyfert galaxies and QSOs. *Nature*, 254:295–298, March 1975.
- [3] J. L. Tonry. Evidence for a central mass concentration in M32. *Astrophysical Journal Letters*, 283:L27, August 1984.
- [4] M. J. Rees. Tidal disruption of stars by black holes of 10 to the 6th-10 to the 8th solar masses in nearby galaxies. *Nature*, 333:523–528, June 1988.
- [5] C. R. Evans and C. S. Kochanek. The tidal disruption of a star by a massive black hole. *Astrophysical Journal Letters*, 346:L13–L16, November 1989.
- [6] L. Hernquist and N. Katz. TREESPH - A unification of SPH with the hierarchical tree method. *Astrophysical Journal Supplement*, 70:419–446, June 1989.
- [7] G. Lodato, A. R. King, and J. E. Pringle. Stellar disruption by a supermassive black hole: is the light curve really proportional to  $t^{5/3}$ ? *Monthly Notices of the Royal Astronomical Society*, 392(1):332–340, 2009.
- [8] J. Guillochon and E. Ramirez-Ruiz. Hydrodynamical Simulations to Determine the Feeding Rate of Black Holes by the Tidal Disruption of Stars: The Importance of the Impact Parameter and Stellar Structure. *Ap. J.*, 767:25, April 2013.
- [9] S. Rosswog, E. Ramirez-Ruiz, and W. R. Hix. Tidal Disruption and Ignition of White Dwarfs by Moderately Massive Black Holes. *Ap. J.*, 695:404–419, April 2009.

- [10] R. V. Shcherbakov, A. Pe'er, C. S. Reynolds, R. Haas, T. Bode, and P. Laguna. GRB060218 as a Tidal Disruption of a White Dwarf by an Intermediate-mass Black Hole. *Ap. J*, 769:85, June 2013.
- [11] R. Haas, R. V. Shcherbakov, T. Bode, and P. Laguna. Tidal Disruptions of White Dwarfs from Ultra-close Encounters with Intermediate-mass Spinning Black Holes. *Ap. J*, 749:117, April 2012.
- [12] S. Kobayashi, P. Laguna, E. S. Phinney, and P. Mészáros. Gravitational Waves and X-Ray Signals from Stellar Disruption by a Massive Black Hole. *Ap. J*, 615:855–865, November 2004.
- [13] T. Bogdanović, R. M. Cheng, and P. Amaro-Seoane. Disruption of a Red Giant Star by a Supermassive Black Hole and the Case of PS1-10jh. *Ap. J*, 788:99, June 2014.
- [14] J. Guillochon, E. Ramirez-Ruiz, S. Rosswog, and D. Kasen. Three-dimensional Simulations of Tidally Disrupted Solar-type Stars and the Observational Signatures of Shock Breakout. *Ap. J*, 705:844–853, November 2009.
- [15] S. Rosswog. Relativistic smooth particle hydrodynamics on a given background spacetime. *Classical and Quantum Gravity*, 27(11):114108, June 2010.
- [16] R. M. Cheng and T. Bogdanović. Tidal disruption of a star in the Schwarzschild spacetime: Relativistic effects in the return rate of debris. *Phys. Rev D*, 90(6):064020, September 2014.
- [17] R.-F. Shen and C. D. Matzner. Evolution of Accretion Disks in Tidal Disruption Events. *Ap. J*, 784:87, April 2014.
- [18] E. R. Coughlin and M. C. Begelman. Hyperaccretion during Tidal Disruption Events: Weakly Bound Debris Envelopes and Jets. *Ap. J*, 781:82, February 2014.
- [19] J. K. Cannizzo. Accretion disks in active galactic nuclei - Vertically explicit models. *Ap. J*, 385:94–107, January 1992.

- [20] J. K. Cannizzo, H. M. Lee, and J. Goodman. The disk accretion of a tidally disrupted star onto a massive black hole. *Ap. J*, 351:38–46, March 1990.
- [21] H. Shiokawa, J. H. Krolik, R. M. Cheng, T. Piran, and S. C. Noble. General Relativistic Hydrodynamic Simulation of Accretion Flow from a Stellar Tidal Disruption. *ArXiv e-prints*, January 2015.
- [22] J. Guillochon and E. Ramirez-Ruiz. A Dark Year for Tidal Disruption Events. *ArXiv e-prints*, January 2015.
- [23] C. Bonnerot, E. M. Rossi, G. Lodato, and D. J. Price. Disc formation from stellar tidal disruptions. *ArXiv e-prints*, January 2015.
- [24] K. Hayasaki, N. C. Stone, and A. Loeb. Circularization of Tidally Disrupted Stars around Spinning Supermassive Black Holes. *ArXiv e-prints*, January 2015.
- [25] E. Ramirez-Ruiz and S. Rosswog. The Star Ingesting Luminosity of Intermediate-Mass Black Holes in Globular Clusters. *Ap. J. Lett.*, 697:L77–L80, June 2009.
- [26] Martin J. Rees. Tidal disruption of stars by black holes of 10 to the 6th-10 to the 8th solar masses in nearby galaxies. *Nature*, 333:523–528, 1988.
- [27] J. Magorrian and S. Tremaine. Rates of tidal disruption of stars by massive central black holes. *Monthly Notices of the Royal Astronomical Society*, 309:447–460, October 1999.
- [28] K. Hayasaki, N. Stone, and A. Loeb. Tidal disruption flares from stars on eccentric orbits. In *European Physical Journal Web of Conferences*, volume 39 of *European Physical Journal Web of Conferences*, page 1004, December 2012.
- [29] J.-P. Luminet and B. Pichon. Tidal pinching of white dwarfs. *Astronomy and Astrophysics*, 209:103–110, January 1989.
- [30] J. E. Dale, M. B. Davies, R. P. Church, and M. Freitag. Red giant stellar collisions in the Galactic Centre. *Monthly Notices of the Royal Astronomical Society*, 393:1016–1033, March 2009.

- [31] N. Stone, R. Sari, and A. Loeb. Consequences of strong compression in tidal disruption events. *Monthly Notices of the Royal Astronomical Society*, 435:1809–1824, 2013.
- [32] Loren I. Petrich, Stuart L. Shapiro, and Saul A. Teukolsky. Accretion onto a moving black hole: An exact solution. *Phys. Rev. Lett.*, 60:1781–1784, May 1988.
- [33] D. N. Burrows, J. A. Kennea, G. Ghisellini, V. Mangano, B. Zhang, K. L. Page, M. Eracleous, P. Romano, T. Sakamoto, A. D. Falcone, J. P. Osborne, S. Campana, A. P. Beardmore, A. A. Breeveld, M. M. Chester, R. Corbet, S. Covino, J. R. Cummings, P. D’Avanzo, V. D’Elia, P. Esposito, P. A. Evans, D. Fugazza, J. M. Gelbord, K. Hiroi, S. T. Holland, K. Y. Huang, M. Im, G. Israel, Y. Jeon, Y.-B. Jeon, H. D. Jun, N. Kawai, J. H. Kim, H. A. Krimm, F. E. Marshall, P. Mészáros, H. Negoro, N. Omodei, W.-K. Park, J. S. Perkins, M. Sugizaki, H.-I. Sung, G. Tagliaferri, E. Troja, Y. Ueda, Y. Urata, R. Usui, L. A. Antonelli, S. D. Barthelmy, G. Cusumano, P. Giommi, A. Melandri, M. Perri, J. L. Racusin, B. Sbarufatti, M. H. Siegel, and N. Gehrels. Relativistic jet activity from the tidal disruption of a star by a massive black hole. *Nature*, 476:421–424, August 2011.
- [34] A. J. Levan, N. R. Tanvir, S. B. Cenko, D. A. Perley, K. Wiersema, J. S. Bloom, A. S. Fruchter, A. d. U. Postigo, P. T. O’Brien, N. Butler, A. J. van der Horst, G. Leloudas, A. N. Morgan, K. Misra, G. C. Bower, J. Farihi, R. L. Tunnicliffe, M. Modjaz, J. M. Silverman, J. Hjorth, C. Thöne, A. Cucchiara, J. M. C. Cerón, A. J. Castro-Tirado, J. A. Arnold, M. Bremer, J. P. Brodie, T. Carroll, M. C. Cooper, P. A. Curran, R. M. Cutri, J. Ehle, D. Forbes, J. Fynbo, J. Gorosabel, J. Graham, D. I. Hoffman, S. Guziy, P. Jakobsson, A. Kamble, T. Kerr, M. M. Kasliwal, C. Kouveliotou, D. Kocevski, N. M. Law, P. E. Nugent, E. O. Ofek, D. Poznanski, R. M. Quimby, E. Rol, A. J. Romanowsky, R. Sánchez-Ramírez, S. Schulze, N. Singh, L. van Spaandonk, R. L. C. Starling, R. G. Strom, J. C. Tello, O. Vaduvescu, P. J. Wheatley, R. A. M. J. Wijers, J. M. Winters, and D. Xu. An Extremely Luminous Panchromatic Outburst from the Nucleus of a Distant Galaxy. *Science*, 333:199–, July 2011.